# Real-time feedback control microscopy for automation of optogenetic targeting

**Lucien Hinderling [1], Alex E. Landolt [1,2], Benjamin Grädel [1,2], Laurent Dubied [1], Cédric Zahni [1], Moritz Kwasny [1], Agne Frismantiene [1], Talley Lambert [3], Maciej Dobrzyński [1], and Olivier Pertz [1,✉]**

[1]Institute of Cell Biology, University of Bern, Baltzerstrasse 4, 3012 Bern, Switzerland
[2]Graduate School for Cellular and Biomedical Sciences, University of Bern, Switzerland
[3]Departments of Systems Biology and Cell Biology, Harvard Medical School, Boston, MA, USA

**Optogenetics have revolutionized our ability to study cellular signaling by enabling precise control of cellular functions with light. Most classical implementations rely on fixed or manually updated illumination patterns, limiting their ability to accommodate for living systems that move, change shape or rapidly adapt their signaling states. Here, we present a real-time feedback control microscopy platform (RTM) that combines automated image segmentation, feature extraction, and adaptive hardware control to dynamically adjust optogenetic stimulation based on live cell behavior. By continuously analyzing biosensor signals, the RTM platform updates illumination patterns in real-time, maintaining region-specific stimulation, inducing traveling activity waves, or selectively activating single cells within a tissue. This fully automated, Python-based framework is built on open standards for microscope control and data handling, supporting large-scale experiments and long-term time-lapse studies. It eliminates the need for human intervention to reposition light patterns or select target cells, thereby enabling reproducible, systematic and high-throughput interrogation of spatiotemporal signaling. Automated and adaptive optogenetic perturbations provide a powerful tool to study how local signaling events shape cellular behavior, from subcellular structures, through single-cell migration, to emergent tissue-level processes.**

**smart microscopy | closed-loop control | optogenetics**
**Correspondence:** ***olivier.pertz@unibe.ch***

## Introduction

Cells are dynamic systems, constantly evaluating and responding to their environment through tightly regulated signaling networks. Traditional representations of signaling pathways oversimplify these processes, ignoring spatial organization, stochastic fluctuations, and mechanical coupling between molecules, organelles, and cells. To fully understand such cellular behavior, researchers must be able to both image but also perturb study signaling in both space and time.

A major challenge in perturbing signaling pathways is cellular adaptation. Long-term genetic and pharmacological perturbations often trigger compensatory mechanisms, making it difficult to isolate direct effects [1, 2]. Feedback loops and crosstalk can restore homeostasis, masking the true role of a given pathway. Optogenetics provides a solution by enabling acute, localized perturbations that do not trigger these compensatory responses. Unlike genetic loss-off-function (knockout, knockdown), or chemical inhibiton approaches that do not allow for precise spatio-temporal control, light-sensitive protein switches allow precise, reversible control of biochemical activities within seconds with micrometer resolution [3, 4].

Due to a lack of adequate technologies, optogenetic experiments still mostly rely on manually selecting regions of interest (ROI) for light stimulation, which prohibits large-scale or long-term dynamic studies. Cells move, change shape, and exhibit heterogeneous behaviors, which makes static illumination patterns ineffective.

To address these limitations, new microscope platforms must integrate real-time feedback and automation into optogenetic experiments. Advances in smart microscopy provide a solution by combining live imaging and computer vision for adaptive light stimulation [5–9][1]. Deep learning-based cell segmentation enables these systems to track and respond to cellular events in real time, allowing fully autonomous experiments based on user-defined rules.

Here, we present a smart microscopy platform for automated optogenetic stimulation across biological scales. Built on open source software, our system analyzes live images to extract cellular features, makes instantaneous decisions, and delivers targeted light stimulation without human intervention. By combining optogenetics with real-time automation, our approach enables experiments that were previously not accessible, offering new insights into dynamic cellular processes. We demonstrate applications across different cellular systems and signaling pathways.

## Results

### Platform for real-time feedback control microscopy

Our experimental platform integrates real-time image processing to track and segment cells while monitoring cell morphodynamics and/or signaling activity measured using biosensors. Based on a specific experiment, we generate a stimulation mask that is projected onto live cells using a digital micromirror device (DMD) for optogenetic activation (fig. 1A). This approach enables dynamic, spatially resolved perturbations, such as maintaining a pattern of

[1]See https://smartmicroscopy.org/literature/ for an up-to-date literature list.

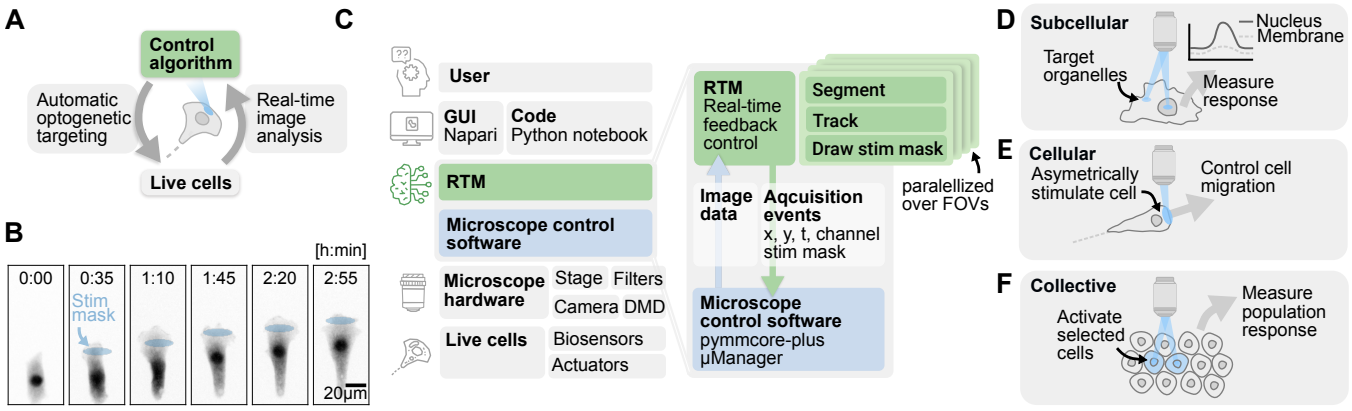


**Fig. 1. Real-time feedback control microscopy for automated optogenetic targeting. A:** Closed-loop control of live cells. Computer vision segments and tracks cells in real time, while a control algorithm generates a stimulation mask to dynamically target specific regions of the cell with light. **B:** Automatically updating the stimulation mask as the cell moves, enables continuous photo activation of a specific cell region. **C:** Overview of the software, hardware, and experimental framework. Users interact with the system through a Napari-based GUI and Jupyter notebooks. The control algorithm includes a modular image processing pipeline and logic for optogenetic stimulation. It communicates acquisition events to the microscope control software (pymmcore-plus / µManager), which manages hardware operation. This modular approach is compatible with various cell lines, biosensors, and optogenetic actuators, making it adaptable to experiments across different biological scales. **D:** Automatic detection of subcellular structures enables targeted perturbations to study heterogeneous signal processing and cytoskeletal feedback within single cells. **E:** At the single-cell level, the platform can induce and control directed migration. **F:** At the tissue level, the system allows precise control over signaling in individual cells or subpopulations, facilitating the study of collective signaling dynamics.

light exposure at the front of a moving cell to induce directed migration (fig. 1B).

Figure 1C provides an overview of the software, hardware, and biological components of our system. Briefly, users interact with the platform through Jupyter notebooks and a graphical interface in Napari. The experiment is controlled through an automated image processing pipeline that acquires images at specific stage positions, processes images, and segments cells using modular computer vision tools that can be adapted for different experimental needs. Our system interfaces with microscope control software through the open source platform µManager [10] and its Python interface, pymmcore-plus [11], allowing integration with various hardware setups.

The modularity of our approach enables compatibility with different cell lines, optogenetic actuators and biosensors, making it adaptable for diverse biological applications. We demonstrate its versatility on multiple scales, from targeting subcellular structures (fig. 1D) to guiding single-cell migration (fig. 1E) and controlling collective MAPK signaling at the tissue level (fig. 1F).

## User interaction and experiment setup

Our platform uses Python and Jupyter notebooks to program, test, and run experiments (fig. 2A). Once a custom workflow is set up, users without programming experience can easily modify parameters directly in the notebook. Its interactivity allows users to preview the image processing pipeline and stimulation logic on live data before starting an experiment. The notebook also serves as automatic documentation, ensuring that all parameters are recorded for reproducibility.

To control the microscope, adjust focus, and select imaging positions in the sample, we use Napari, a Python-based multidimensional image viewer [12], as a graphical user interface. The napari-micromanager plugin provides a user-friendly interface for routine microscope operations. Additional Napari plugins or custom widgets can be easily integrated, for example, to calibrate the DMD or interactively train image segmentation tools on live data.

Once an experiment is running, data is continuously stored using OME-Zarr [13], along with a data table for additional extracted data (fig. 2B). The data, including segmentation overlays, tracking information, and stimulation masks, can be visualized in Napari for real-time quality control. This immediate feedback simplifies troubleshooting and reduces iteration time when an experiment fails (fig. 2C). Since data is processed during the experiment and available immediately after, there is no need for additional feature extraction steps, streamlining post-experimental analysis.

## Image processing pipeline

Our experiments rely on real-time image processing to generate segmentation masks, track cells, quantify biosensor activity, and detect ROIs for photoactivation. We selected Python for implementing feedback logic and image/data analysis because of its comprehensive libraries for computer vision and signal processing. A modular framework allows to easily replace individual components in the processing pipeline. Each frame is processed in a separate background thread while the main thread continues to acquire new data.

Cell appearance can vary significantly between experiments, as morphology and biosensor signals can be strongly affected by factors such as drug treatments, making pretrained segmentation models unreliable. To address this, we developed Convpaint, an interactive pixel classifier that users can train for cell segmentation in about one minute using a single representative image taken directly from live data before starting an experiment (detailed in a separate publication [14]). For cell lines with stable cell

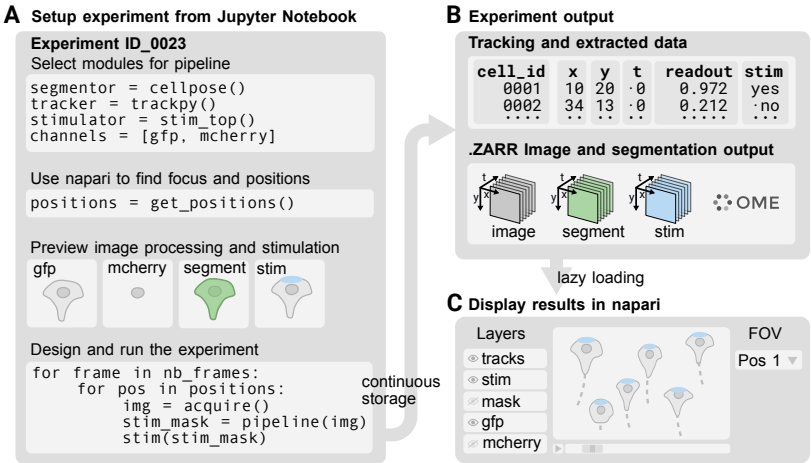


**Fig. 2. Experiment setup, data output, and visualization. A:**Experiments are set up in Jupyter notebooks, with step-by-step instructions and an interactive preview of the image processing pipeline. This allows researchers, even without coding experience, to customize and run experiments. **B:** During the experiment, data is continuously stored. Tracking data and other quantitative measurements are saved as pandas DataFrames, while image data and masks are stored in OME-Zarr format. **C:** The output can be directly visualized in Napari, enabling easy troubleshooting during experiments and streamlined analysis of results.

appearance, pretrained segmentation models can be easily integrated into our platform. We use StarDist [15] for segmenting nuclear markers and Cellpose3 [16] for segmenting cells that express cytosolic markers.

To accommodate microscope computers with older hardware, we integrate the Imaging Server Kit [17], allowing segmentation tasks to be offloaded to more powerful remote workstations or servers. The Docker-based deployment facilitates quick setup and execution while isolating dependencies, thereby avoiding package conflicts between projects or analysis modules. Microscopy images are transferred to a remote web server via a FastAPI-based web interface, and the resulting segmentation masks are returned to the RTM pipeline.

Cell tracking is performed building on the trackpy library [18], which allows new image frames to be added incrementally without reprocessing previous frames. Other tracking tools, such as btrack [19], are also compatible with our pipeline.

Our pipeline extracts quantitative data, including morphodynamic features such as cell shape, migration speed, as well as signaling activity extracted from biosensor images, enabling targeted stimulation based on live analysis. For example, it can selectively stimulate cells with a specific signaling state or those matching a specific morphology. The data extraction process is highly customizable, users can add their own features by providing any Python function that extracts information from the image, segmentation mask and/or tracking data, and returns the information as a dataframe.

The biological processes we studied occur on relatively slow timescales, with image acquisition intervals of at least 10 seconds. In all experiments, throughput was limited by hardware constraints (stage speed, filter wheel switching time, and camera exposure time) rather than image processing speed. To illustrate throughput, a 20x objective provided sufficient resolution to simultaneously control approximately 250 sparsely seeded cells across 24 fields of view at two-minute intervals. In high density epithelial monolayers, we successfully tracked 10'491 cells simultaneously (12 fields of view, 2 min resolution). Although rapid response times were not required for our biological experiments, we tested the system's ability to quickly process images and respond to detected features. In a proof-of-concept experiment, we achieved response times below 1 second, including image acquisition, basic image processing (otsu thresholding, watershed segmentation), mask generation, and hardware adjustments. Also in this case the filter wheel changes were the limiting factor, and could easily be improved by using a dichroic mirror compatible with stimulation and acquisition wavelengths.

## Hardware-software integration

Smart microscopy solutions developed in academic labs often encounter interoperability issues because microscope programming interfaces differ significantly between vendors or may be closed-source. Community initiatives such as `www.smartmicroscopy.github.io` aim to develop standardized interfaces to address these issues. In this project, we adopted the hardware-agnostic *useq-schema* [20] to describe image acquisition events: Instead of directly specifying hardware commands, useq-schema defines metadata of acquisition events, such as positions, time points, and imaging channels. The microscope control software then translates this metadata into specific hardware instructions. This approach allows to abstract the experiment logic from the underlying microscope hardware used. For example, different cameras or DMDs, such as the Andor Mosaic 3 and Mightex Polygon 1000, can be used interchangeably, without requiring any change in the code. *Useq-schema* integrates effectively with pymmcore-plus, providing access to µManager's extensive library of microscope hardware drivers. µManager hosts the largest collection of device drivers and is widely adopted, making our method compatible with a wide range of existing microscope setups.

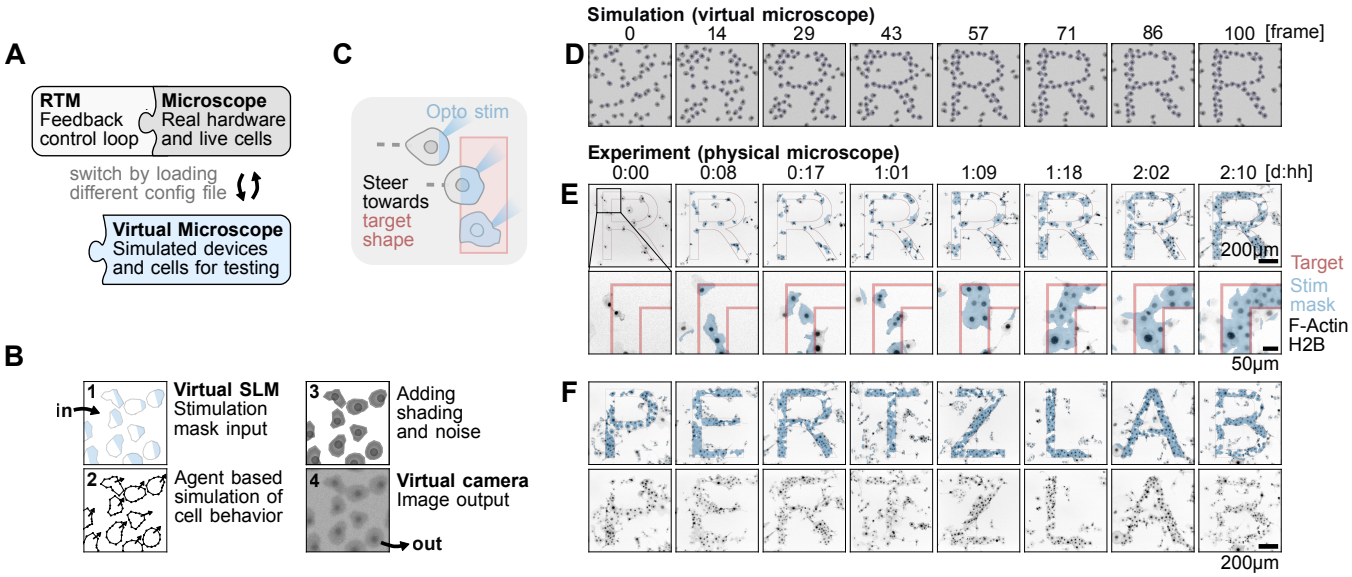


**Fig. 3. Virtual microscope and feedback-controlled patterning of multicellular structures. A:** Switching between real and virtual hardware enables seamless testing and debugging of closed-loop microscopy pipelines. **B:** Simulation pipeline: the stimulation mask drives cell behavior in the agent-based model; the resulting cell positions are rendered and processed to resemble microscopy images, allowing *in silico* testing of feedback control workflows. **C:** Experimental goal: guide cells towards a user defined shape and maintain them there once they have reached their location. Once the shape is sufficiently occupied, remaining cells in the FOV are steered away from the pattern to increase contrast. **D:** Time series from simulation showing cells to the target pattern. 100 frames were simulated in 13 seconds. **E:** Time series from the corresponding experiment, showing cells gradually forming the same target pattern over several days. Towards the end of the experiment, excess cells are steered away from the pattern. Cells express optogenetic TrkA actuator, biosensors for F-Actin (Lifeact) and nucleus (H2B). **F:** Example of patterned tissues using the feedback approach; shown are the eight best FOVs and frames manually selected from 24 FOVs of a single experiment.

## Virtual microscope for testing closed-loop experiments

Microscopy control scripts are often tested with virtual "fake cameras" that replay pre-recorded images. While sufficient for non-feedback pipelines, such cameras cannot react to perturbations, making it impossible to test feedback control. To overcome this limitation, we developed a virtual microscope that simulates a simple cell model responding to light stimulation. Built on the UniMMCore framework of pymmcore-plus, the system allows seamless switching between physical and simulated devices by simply loading a different hardware configuration file, while keeping all device APIs identical. This enables users to develop, test, and debug microscopy experiments in a virtual environment, as well as create and control new (simulation) devices entirely in Python. This setup allows researchers to test imaging strategies, feedback loops, and analysis in silico, and to systematically verify workflows before carrying out real experiments, which can be time-consuming and costly (fig. 3A).

As a test case, we simulated how cells would behave if they expressed an optogenetic tool that induces local protrusions and directional motility. We use a agent-based simulation, using a vertex-based representation. Each cell is modeled as a deformable polygon whose vertices fluctuate under Brownian noise (random displacements of vertices each update, producing jittery, diffusive motion), curvature relaxation (smoothing force that evens out the cell boundary, counteracting sharp angles and restoring roundness), and area conservation. When a stimulation mask is provided, vertices overlapping illuminated pixels protrude outward from the cell centroid and the whole cell receives a directed impulse toward the stimulated side. Cells interact through collisions under periodic boundaries. The scene is rendered as shaded polygons and passed through a contrast, blur, noise, and brightness filter to resemble a microscope image (fig. 3B). We used the simulation to develop an experiment where the goal was to assemble cells into a target shape. The virtual microscope allowed us to quickly iterate over different stimulation rules. In the final code, each cell is guided based on how much it overlaps with the target: cells that don't overlap are steered toward the unoccupied areas of the target shape, cells with partial overlap are steered toward a locally expanded portion of the target, and cells that already overlap enough are only stimulated in the overlapping region. Once the overall occupancy crosses a threshold, the rules switch to a mode that keeps cells already on the pattern in place, while pushing all other cells away from the target shape (fig. 3C,D).

We then implemented the same stimulation rules in experiments with real cells to test whether the simulated behavior could be reproduced in practice . Using a 3.5-minute interval, we could run 24 fields of view in parallel and guide NIH3T3 fibroblasts, expressing an optogenetic TrkA receptor, to assemble into letter shapes (fig. 3E,F). While in the simulator the cells converged to the target pattern within seconds, in the actual experiment the process took several days.

To study collective cell behavior in colonies of defined sizes and the influence of geometry on signaling, microcontact printing of adhesive and non-adhesive proteins on glass has been used. The approach presented here could serve as a form of "dynamic micropatterning", enabling the

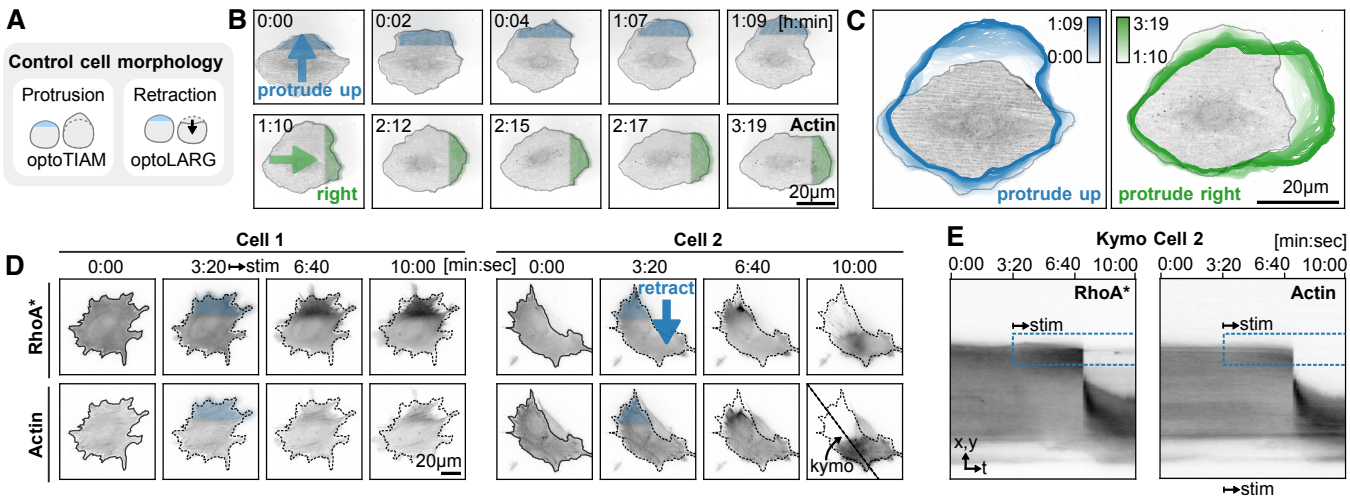


**Fig. 4. Optogenetic perturbations to control cell shape and migration at the single-cell scale. A:** Controlling protrusion and retraction using optogenetic tools for Rac (optoTIAM) and RhoA (optoLARG). **B:** The cell is segmented with Convpaint using an F-actin biosensor image. Light is first projected onto the top of the mask to activate optoTIAM, inducing protrusions in that direction. After 1:09 (h:min), stimulation switches to the right side, and the cell redirects protrusions accordingly. **C:** Cell outlines over time show shape deformation. The left panel (0:00 to 1:09 h:min) captures the cell moving upward, while the right panel (1:10 to 3:19 h:min) shows movement to the right. **D:** Cells expressing the optogenetic RhoA actuator (optoLARG) are segmented using Convpaint (dashed outline). The top region is automatically selected for repeated stimulation (projected light shown as a blue overlay on the first stimulation frame), leading to local accumulation of RhoA* and F-actin, followed by retraction of the stimulated area. Line labeled kymo indicates location of kymograph in E. **E:** Kymograph showing gradual buildup of RhoA* and F-actin at the illuminated edge, then spring-like retraction in the Cell 2. Blue box indicates stimulated area.

assembly of cells into shapes that move or change over time. Traditional micropatterning methods cannot adapt to cell heterogeneity or variability in seeding, making it difficult to seed an exact number of cells to a pattern. In contrast, the feedback-control approach demonstrated here allows precise control over individual cells, and could be used to ensure a specific number of cells in each collective. This approach could act as a "tissue printer", dynamically arranging cells into defined shapes and sizes without fixed physical scaffolds. Guiding and reshaping cell groups over time, it could offer a flexible way to build multicellular structures for studying development or creating custom-designed tissues.

In the next section, we show additional applications of the platform across different biological scales and pathways, focusing more on the biological rather than the technical details of the experiment presented here.

## Experimental applications of the platform

### Subcellular control of Rho GTPase signaling

Cytoskeletal dynamics are regulated by Rho GTPases [22], which are themselves controlled by GEFs (guanine nucleotide exchange factors) and GAPs (GTPase-activating proteins)[23]. The large number of GEFs and GAPs, many with partially redundant functions, makes traditional genetic loss-of-function studies challenging. Moreover, emerging evidence indicates the presence of feedback mechanisms that result in complex signaling dynamics, including localisation to specific cytoskeletal structures [24], responses to mechanical forces [25], or propagating signaling waves at the cellular cortex [26]. Overexpression studies have found three canonical RhoGTPases, which regulate contractility (RhoA), protrusion formation (Rac), or filopodia (CDC42) [27]. This dogma is challenged by paradoxical observations reported by imaging studies, such as RhoA activity involved in protrusions [28, 29], deactivation of RhoA by Rho GEFs depending on the concentration of the GEFs [30], or RhoA involved in the regulation of actin disassembly [31], and reveal the complexity and fine-tuned spatio-temoral patterning of these regulatory networks. Optogenetics in combination provides a powerful method to investigate such intricate dynamics [30, 32]. Here we show how RTM can leverage optogenetic approaches for such experiments to control cell shape, automatically target cytoskeletal structures, and produce signaling patterns with spatial dynamics to replicate phenomena such as propagating waves. Using optogenetic actuators for two different Rho GTPases, Rac and RhoA, we can induce cell protrusion or contractility, respectively, in rat embryonic fibroblast cells (REF52). The two actuators work by recruiting the catalytic domain of a Rho-specific GEF to the stimulation location, locally activating the Rho GTPase (optoLARG for RhoA, optoTIAM for Rac, fig. 4A). As readout, we show different cytoskeletal biosensors, marking active RhoA (RhoA*, 2xrGBD::dTomato), focal adhesions (paxillin::mCherry) and actin fibers (Lifeact::miRFP). To form protrusions with optoTIAM in a controlled direction, the cell was continuously segmented and the stimulation mask was dynamically updated to account for morphological changes over time (fig. 4B,C). Using automated stimulation of optoLARG (optoLARG::mVenus::SspB(nano)::p2A::iLID::CAAX), we could make cells systematically contract on one side (fig. 4D).

**Targeting of subcellular structures).** Here we demonstrate automated optogenetic targeting at subcellular resolution, examining RhoA* response at specific cellular locations, here focal adhesions. While in the previous example, we

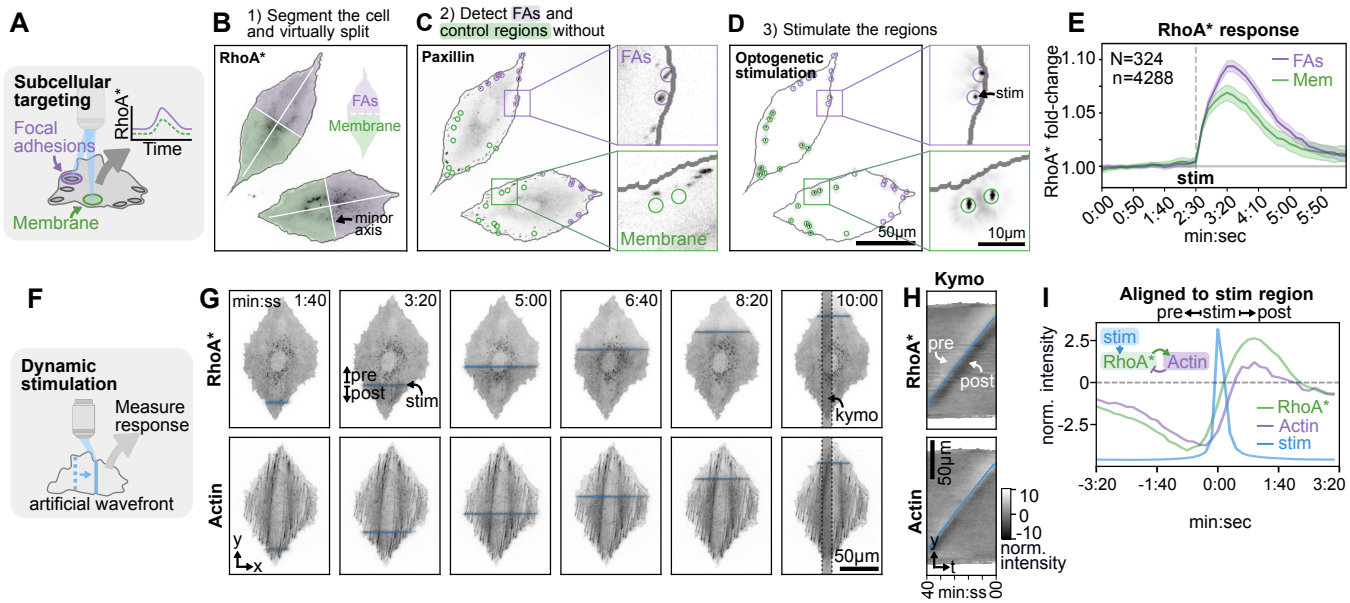


**Fig. 5. Automatic targeting of subcellular structures and dynamic stimulation patterns.** **A:** RhoA is locally activated using an optogenetic GEF (optoLARG) at focal adhesions and membrane regions without focal adhesions. Local RhoA activity (RhoA*) is measured using a fluorescent biosensor in the stimulated regions. **B:** The cell is segmented using Convpaint on the RhoA* channel and virtually divided along the minor axis. One side is stimulated at focal adhesions, the other at membrane regions, allowing for within-cell controls. **C:** Regions selected for stimulation are marked with circles. **D:**Image of the projected light pattern for optogenetic stimulation. Stimulation spots are micron-sized. **E:**The process is fully automated, enabling the screening of thousands of stimulation regions (n = 4'288) across hundreds of cells (N = 324). Median and 99% CI are shown. RhoA* shows stronger response at focal adhesions than at the membrane, indicating cytoskeletal feedback on RhoA* signaling. Data is pooled from four technical replicates and was previously reported in [21]. **F:** A line scan induces an artificial wave of signaling activity using optoLARG. RhoA* and F-actin are measured using fluorescent biosensors. **G:** Time series showing RhoA* and F-actin recruitment after stimulation. An image of the projected light pattern is overlaid in blue. Stimulation line width is 1.3 µm (half-height width of the peak-profile). **H:** Kymograph averaged over a 50-pixel-wide region across all time points. Data is corrected for photobleaching and structural background, then normalized to mean expression levels. The blue line indicates the y-position of the stimulation mask centroid. RhoA* depletion is observed ahead of the stimulation line, while an increased biosensor signal appears behind it. **I:** Kymograph data aligned to the y-centroid of the stimulation mask, showing dynamics of RhoA* and actin as function of time relative to peak optogenetic activation. The light stimulation profile is manually rescaled and offset for visualization. Scheme shows hypothetical regulatory network that could explain these dynamics.

induced strong morphological changes, we now instead apply a much more subtle stimulation, with no visible effect on cell shape. Automated targeting of specific cytoskeletal structures enables to systematically probe cytoskeletal feedback onto RhoA* (fig. 5A), a technique we previously applied to study the role of DLC1 in actin regulation [21]. The cells are segmented using Convpaint on the RhoA* channel, then virtually divided into two regions (fig. 5B): In one half, small regions at focal adhesions are selectively activated, while in the other half, regions between focal adhesions are targeted (fig. 5C). The focal adhesions are detected using the paxillin channel, the non-focal adhesion regions are selected by sampling from regions close to the cell edge, with a minimum distance to focal adhesions (fig. 5D). This method provides automated control within the same cell. By automatically actuating and measuring RhoA* in thousands of focal adhesions and membrane regions without focal adhesions, we identified distinct spatial activity patterns, suggesting differential regulation by GEFs and GAPs depending on local cytoskeletal context: Positive feedback from focal adhesions on RhoA* signaling. The results of this high-throughput experiment are shown in fig. 5D and were previously published in [21]. Initial attempts using strong optogenetics hid this spatial heterogeneity because of cytoskeletal remodeling, and were only revealed when using subtle, transient stimulations that slightly disrupt the equilibrium. These weak perturbations operate in a regime with low signal-to-noise ratio, and required high-throughput experiments enabled by RTM automation to achieve statistical significance.

**Simulating subcellular signaling waves.** Reaction-diffusion systems on the cell cortex generate distinct patterns such as clusters [33] or waves [26] observed in frog oocytes [34], dictyostelium [35], and REF52 cells [36]. These dynamic waves serve diverse functions, regulated by their spatio-temporal dynamics. To investigate these functions, we sought to artificially induce RhoA* signaling waves using optoLARG, by replicating the spatial and temporal characteristics of naturally occurring waves (fig. 5F). Cells are segmented on the RhoA* channel, and a thin stimulation line is scanned from bottom to top (fig. 5G). A kymograph of this data, after detrending and normalization, reveals a distinct intensity band trailing the stimulation line for both RhoA* and F-actin, while a band of decreased intensity appears ahead of the wavefront (fig. 5H).

Aligning the measurements to the stimulation region and averaging allows a direct comparison of RhoA* and actin dynamics over time. RhoA* precedes F-actin by 30 seconds (three frames) during recruitment, but both reach peak activation simultaneously. After the peak, RhoA* decays at a faster rate than F-actin. These dynamics suggest a regulatory loop where optogenetic activation of RhoA* promotes F-actin polymerization, which in turn inhibits RhoA* (fig. 5I), possibly through recruitment of a

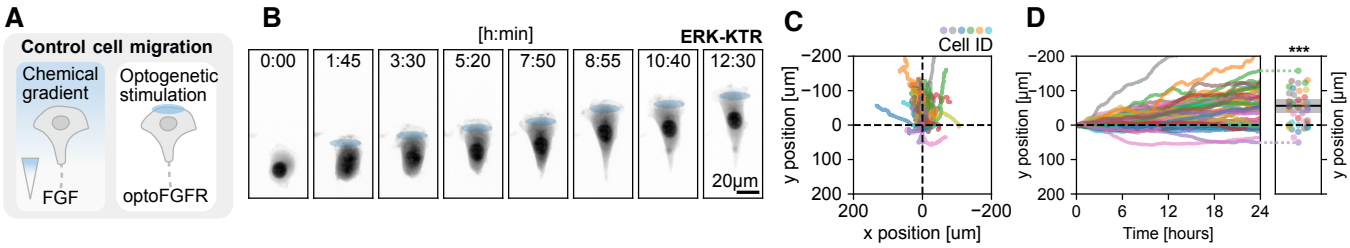


**Fig. 6. A:** To study migration in response to growth factor gradients, artificial asymmetric growth factor input is created using optogenetics. NIH3T3 cells expressing optoFGFR are tracked and periodically stimulated with an elliptical mask offset from the nuclear centroid. **B:** Example of a single cell showing polarization and directed migration in response to stimulation. **C:** Cell trajectories normalized to their initial positions to assess net displacement. **D:** By 24 hours, cells exhibited a significant shift in the y direction (–56.03 ± 68.66 µm, $p = 2.60\times10^{-6}$, t = –5.41, df = 43), while displacement in the x direction remained non-significant (–3.00 ± 36.73 µm, p = 0.59, t = –0.54, df = 43). These results indicate a directional migration response to the optogenetic stimulation.

Rho GAP as previously observed [37–39]. An unexpected use of this system was that we could use the controlled wave signal as ground-truth reference to calibrate a computer vision algorithm to detect spatially coordinated cellular dynamics [36]. Although wavelike optogenetics has been applied at larger scales [40–42], to our knowledge, this is the first demonstration of artificially replicating subcellular signaling waves. This emphasizes the potential of RTM for future studies of Rho GTPase signaling, using standardized spatio-temporal perturbations in robust, high-throughput assays.

## Single-cell scale control of RTK signaling

We also considered optogenetic perturbations of the cell as a whole, analyzing its mechanochemical behavior as a single integrated unit. To understand how cells achieve directed migration, a key focus is how they regulate protrusion and retraction dynamics to break symmetry. Cells can detect shallow growth factor gradients and amplify them into polarized signaling responses. Using optogenetics, we can provide asymmetric stimulation to cells and study the resulting symmetry breaking and polarization.

**Directing migration.** Cells interpret chemotactic growth factor gradients by generating steeper intracellular signaling gradients, which drive directed migration towards the growth factor source. To investigate this behavior, we induced asymmetric RTK signaling by optogenetically activating an optogenetic fibroblast growth factor receptor (optoFGFR::mCitrine [43]) with light exposure localized on one side of the cell (fig. 6A). We observed cells (mouse embryonic fibroblasts, NIH3T3) migrating toward the illuminated region and using RTM continuously updated the stimulation position to maintain the directional cue (fig. 6B). Previously requiring manual adjustment of illumination regions [44], using our automated method, we can now simultaneously control directional migration of hundreds of cells. This significantly enhances the throughput and reproducibility of gradient sensing studies. Passmore et al. [9] has recently demonstrated automated migration control with an optogenetic actuator for Rac.

## Controlling collective signaling dynamics

We demonstrate applications of RTM at the tissue level, perturbing the dynamics of ERK signaling using 2D epithelial sheets derived from human breast cells (MCF10A cells). Collective ERK signaling in tissues plays a critical role in wound healing, morphogenesis, and cancer biology. These observations rely on imaging studies that provide single-cell-level activity time series. Optogenetic experiments with static illumination shapes have been applied to whole populations or subgroups of cells, and have shown to be effective in untangling the spatial components of emergent behaviors such as collective movement [45]. As cells move in tissue, optogenetic control of specific cells requires tracking and adaptive stimulation patterns. We demonstrate that RTM enables phototargeting of single cells during long-term experiments, and how we can use biosensor data extracted during the live experiment to control a cell's activity based on its previous signaling history. This closed-loop control is essential to identify causal relationships in collective behavior. In the next experiments we use a optogenetic biosensor-actuator circuit in MCF10A cells [43], with a nuclear marker to track (Histone 2B::miRFP703), an ERK-KTR biosensor to measure ERK activity (ERK KTR::mRuby2), measuring the ratio of cytosolic versus nuclear fluoerescence intensity, and an optogenetic fibroblast growth factor receptor (optoFGFR::mCitrine) that allows activation of ERK, or optoLARG to trigger cell contractility. To automatically quantify single-cell ERK activity, a multi-step image processing pipeline is used [46].

**Inducing apoptosis in specific cells.** Epithelial tissues preserve integrity through apoptosis-induced survival: When a cell dies, neighboring cells receive a transient ERK pulse that protects them from apoptosis for several hours. This mechanism prevents multiple nearby cells from dying simultaneously and forming holes in the epithelium [47]. Because spontaneous apoptosis is rare, prior studies often relied on chemotherapeutic agents to trigger cell death, affecting the health of the entire tissue. RTM enables a more targeted approach: by targeting cells with a spot of UV light over several hours (standard 395nm LED in our fluorescence microscope), we induce photo damage leading to cell death (fig. 7A). The targeted nuclei shrink and are extruded from the epithelium (fig. 7B). Note that the progression does not follow classical apoptosis, there is no blebbing, chromatin condensation, or fragmentation into apoptotic bodies, but still triggers a radial ERK activa-

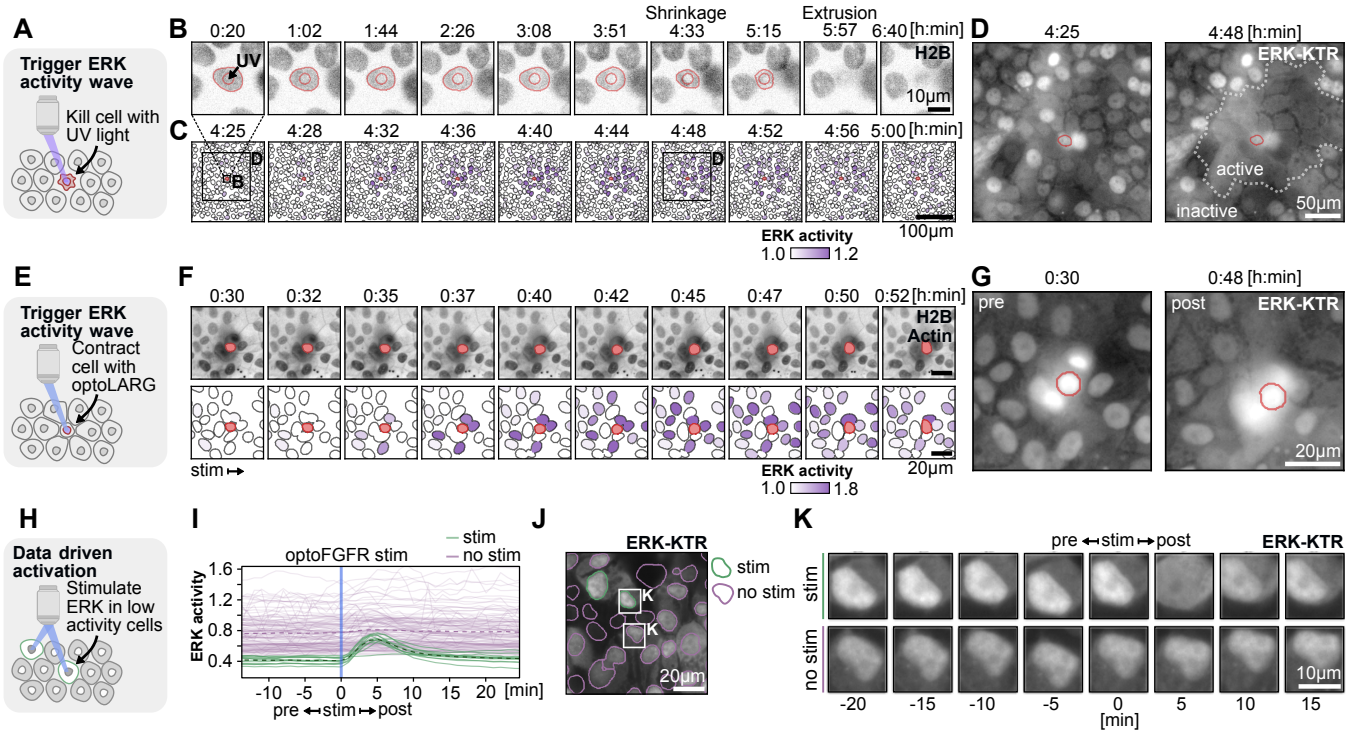


**Fig. 7. Applications of RTM at the tissue scale.** MCF10A cells grown in a confluent monolayer express a nuclear marker for tracking (H2B), an ERK activity biosensor (ERK-KTR), and an optogenetic FGF receptor (optoFGFR) or optoLARG. **A:** A single cell is tracked and continuously exposed to UV light to investigate how surrounding cells respond to cell death. **B:** Time series centered on the selected cell, showing its mask and the stimulation area (small circle, 5 µm diameter). Bleaching is visible in the stimulation region, followed by nuclear shrinkage and cell extrusion from the epithelium. **C:** A larger view of the epithelium displaying the segmentation mask (black) and color-coded ERK activity (purple, ERK-KTR cytosol/nuclear ratio, normalized to 4:20 h:min). The UV-exposed cell is marked in red. The time series captures ERK dynamics around nuclear shrinkage, revealing an ERK activity wave propagating outward from the selected cell. The small inset at 4:25 h:min indicates the crop size used in B (but from a different time point). The large insets at 4:25 and 4:48 h:min correspond to crops shown in D. **D:** ERK-KTR signal before (4:25 h:min) and at peak ERK activity (4:48 h:min). The area of activated cells (biosensor translocated from nucleus to cytosol) is outlined with a dashed line. **E:** A cell with high optoLARG expression is detected and stimulated to contract, causing an ERK activity wave in neighboring cells. **F:** Timeseries showing nuclear marker and actin stain (top row) and ERK activity (bottom row, normalized to 0:00 h:min). Stimulation starts at 0:30 and is repeated every 15 sec. An ERK-activity wave spreads from the selected cell. **G:** ERK-KTR signal before first stimulation (0:20 h:min) and at peak ERK activity (0:48 h:min). **H:** ERK activity is monitored in real time and used to guide optogenetic ERK activation via optoFGFR. Cells in the lowest 0.1 quantile of integrated ERK activity are selected for stimulation. **I:** ERK activity (ERK-KTR cytosol/nuclear ratio) plotted over time. Cells with low ERK activity (green) are selected for optogenetic activation. Following stimulation, activated cells exhibit a pulse of ERK activity, whereas unstimulated cells show only a slight increase (mean activity per group indicated by a dotted line. **J:** ERK-KTR channel image with cell outlines colored to indicate selection for stimulation. Two cells in close proximity from either class are shown in detail in H. **K:** Time series of two neighboring cells, one selected for stimulation and one not. The stimulated cell shows translocation of the ERK-KTR biosensor to the cytosol upon activation, while the unstimulated cell exhibits no change in biosensor distribution.

tion wave in neighboring cells, similar to those seen during natural apoptotic events. In one experiment, the wave reached more than 20 cells (fig. 7D), although typical responses involved fewer than 10. Because we control the location of death events, we can optimize the field of view, avoid edge artifacts, and increase the yield of informative events without compromising overall tissue health.

**Inducing ERK activity wave using optoLARG.** We asked whether the local mechanical contraction of apoptotic cell extrusion is sufficient to drive an ERK wave. To test this, we mimicked contraction using MCF10A cells expressing optoLARG. Using RTM, we automatically identified the cell with the highest expression of optoLARG, which would generate the strongest contraction upon light activation. We then stimulated this cell with a 32 µm diameter spot every 15 seconds after a baseline of 30-minute (fig. 7E). This induced rapid contraction of surrounding tissue toward the targeted cell, followed by an outward-propagating wave of ERK activity (fig. 7F,G).

**Stimulating cells based on signaling history.** Epithelial homeostasis and other collective dynamics are emergent behaviors that arise from stochastic single-cell signaling and cell-cell communication. To better understand such phenomena, our goal is to re-engineer them by artificially controlling single-cell signaling activity. In this proof-of-concept experiment, we show that we can control single-cell ERK activity, taking into account the previous signaling history. We measure ERK activity timeseries and then selectively activate the cells with the lowest integrated activity using optoFGFR (fig. 7H). Stimulated cells exhibit a strong ERK activity pulse, while non-selected cells generally show flat activity, with few exceptions (fig. 7I). One possible explanation for ERK responses in non-selected cells is that overlapping protrusions may expose multiple cells to light when a single point is illuminated. Another factor could be non-uniform optoFGFR expression (we previously observed differences exceeding 30-fold [43]), where some cells express the actuator at high levels and respond even to small amounts of scattered or diffracted light. This issue could be addressed through FAC sorting or alterna-

tive genetic engineering approaches. Fig. 7J and K show a representative time series of two neighboring cells, one selected for activation and one not.

These examples demonstrate first steps towards artificially engineering collective signaling dynamics, and the RTM system's ability to run complex image processing pipelines to extract real-time activity data, used to perturb the sample in a data drive fashion.

## Discussion

We demonstrate a real-time feedback control microscopy (RTM) platform that enables automated optogenetic perturbations, eliminating the need for manual intervention to stimulate biological targets. By integrating automated segmentation, tracking, and stimulation logic into an open source modular framework, we provide an adaptable system to study dynamic cellular processes across multiple biological scales. The system is robustly tracking cells or subcellular structures over long time periods and precisely stimulates targets at the micrometer scale. RTM enables researchers to reproducibly manipulate and interrogate signaling pathways with throughput previously inaccessible.

**Technical implementation.** Currently, commercial solutions for automating microscopy using image feedback do not match the requirements from academic research labs, prompting the development of custom software solutions. These implementations are often developed for highly specific experimental needs, leading to a fragmented ecosystem of custom-built tools. We aimed to make our software as compatible with other soft and hardware as possible, and contributed to existing open source projects to enable DMD based targeting with the existing uManager / pymmcore-plus / useq-schema software stack instead of developing custom workarounds. This in turn has the benefit that our software is interoperable with other hardware devices already implemented in this system, ensuring compatibility across a wide range of hardware setups, simplifying adoption, and enabling long-term sustainability. Our adoption of useq-schema as a hardware-agnostic acquisition event description format marks a step toward standardization of smart microscopy approaches, with the hope that other platforms will adopt this approach to enhance interoperability and reduce the fragmentation that currently exists. Standardized experiment definitions would allow researchers to seamlessly switch between different microscope systems, making experimental protocols more portable and reproducible. Using OME-Zarr as image format enhances integration with other downstream data analysis tools.

**Customizability vs. ease-of-use.** There is an inherent trade-off between customizability and ease-of-use. We tried to strike a balance by focusing on the task of automating optogenetic targeting and modularizing components like image segmentation, tracking, and stimulation logic, allowing researchers to tailor the RTM system to their specific research question.

A key advantage of our setup is the tight integration with the Napari image viewer, providing a graphical interface for experiment setup, real-time visualization, and quality control. While for initial setup of an experiment coding is required, for subsequent experiments this integration also enables researchers with limited programming experience to run their own experiments. By separating the experiment logic from the data handling code, the experimental logic can also be more easily customized with the help of LLM coding assistants, lowering the entry barrier for advanced customization.

**Use cases.** Our approach is compatible with various optogenetic actuators and biosensors, allowing applications in different model systems, from single cells to tissues. While our primary focus is on optogenetic control, our platform is compatible with any light-based perturbation system, one example we demonstrate is to induce cell death in specific cells just by shining UV light. We also use the same UV projection setup for microfabrication [48], highlighting potential uses of the platform beyond cell biology.

**Future directions.** Currently, our system follows preprogrammed experimental logic, where the user defines the segmentation, tracking, and stimulation rules in advance. The next step in the evolution of smart microscopy is the integration of active learning approaches. By incorporating statistical models that autonomously detect patterns or outliers, the system could dynamically adjust experimental parameters based on [49]. Similar approaches have been successfully applied in chemistry and material sciences [50, 51], where autonomous experiments iteratively refine hypotheses by selecting optimal perturbations based on real-time analysis. In biology, this could translate to experiments that automatically identify rare or unexpected cellular responses, adjusting stimulation parameters to probe the underlying mechanisms in real-time. For example, a system could track fluctuations in signaling activity and adapt stimulation patterns to maximize information gain rather than rely on predefined rules.

A future avenue to explore is LLM based microscope control. LLMs are being used successfully in robotics, as a user interface [52], for task planning [53], perception, and decision making [54]. Modern microscopes are imaging robots: Bridging the gap between LLMs in robotics and biology could make complex microscopy experiments accessible to a wide audience simply by describing the experiment in natural language.

**Conclusion.** Our platform represents a step toward fully autonomous smart microscopy, providing an open, modular, and standardized framework for real-time optogenetic feedback control. By integrating segmentation, tracking, and stimulation logic into a single system, we enable reproducible and scalable optogenetic experiments across biological scales. The open source nature of our approach

ensures long-term sustainability, while its modularity allows easy adaptation to diverse research needs. Looking forward, the integration of active learning methods will further enhance the platform's capabilities, enabling truly autonomous experimental design and execution.

## Code availablability

The RTM software is open source (MIT license) and hosted on GitHub: https://github.com/pertzlab/rtm-pymmcore. The simulation code is not yet merged into the main repo, and currently available from https://github.com/hinderling/opto-loop-sim.


### ACKNOWLEDGEMENTS

This work has been supported by the Chan Zuckerberg Initiative (CZI) grant NP2-0000000095 to LH and OP, grant by the Digitalisierungskommission (Digi-K) of the University of Bern to LH, Uniscientia fellowship 187-2021 to OP, SNF Sinergia grant CRSII5_183550 to OP, Novartis Foundation grant #20C219 to OP, Faculty of Sciences of the University of Bern grant to OP, and Schweizerischer Nationalfonds (SNF) grant 310030_185376 to OP. Microscopy experiments were performed on equipment supported by the Microscopy Imaging Center (MIC), University of Bern, Switzerland.


### AUTHOR CONTRIBUTIONS

LH, AL, BG and TL developed software. LH, LD and MK performed experiments. CZ established optoTrkA cell line. LH analyzed data and created the figures. LH and OP wrote the paper and acquired funding. AF, MD and OP supervised the work.

### COMPETING FINANCIAL INTERESTS

The authors declare that they have no conflict of interest.

# Bibliography


[1] Mohamed A. El-Brolosy and Didier Y. R. Stainier. Genetic compensation: A phenomenon in search of mechanisms. *PLOS Genetics*, 13(7):e1006780, July 2017. ISSN 1553-7404. doi:10.1371/journal.pgen.1006780.

[2] Chong Sun, Liqin Wang, Sidong Huang, Guus J. J. E. Heynen, Anirudh Prahallad, Caroline Robert, John Haanen, Christian Blank, Jelle Wesseling, Stefan M. Willems, Davide Zecchin, Sebastijan Hobor, Prashanth K. Bajpe, Cor Lieftink, Christina Mateus, Stephan Vagner, Wipawadee Grernrum, Ingrid Hofland, Andreas Schlicker, Lodewyk F. A. Wessels, Roderick L. Beijersbergen, Alberto Bardelli, Federica Di Nicolantonio, Alexander M. M. Eggermont, and Rene Bernards. Reversible and adaptive resistance to braf(v600e) inhibition in melanoma. *Nature*, 508(7494):118–122, March 2014. ISSN 1476-4687. doi:10.1038/nature13121.

[3] Matthew J Kennedy, Robert M Hughes, Leslie A Peteya, Joel W Schwartz, Michael D Ehlers, and Chandra L Tucker. Rapid blue-light–mediated induction of protein interactions in living cells. *Nature methods*, 7(12):973–975, 2010.

[4] Lukasz J Bugaj, Atri T Choksi, Colin K Mesuda, Ravi S Kane, and David V Schaffer. Optogenetic protein clustering and signaling activation in mammalian cells. *Nature methods*, 10 (3):249–252, 2013.

[5] Diane-Laure Pagès, Emmanuel Dornier, Jean de Seze, Emilie Gontran, Ananyo Maitra, Aurore Maciejewski, Li Wang, Rui Luan, Jérôme Cartry, Charlotte Canet-Jourdan, Joël Raingeaud, Grégoire Lemahieu, Marceline Lebel, Michel Ducreux, Maximiliano Gelli, Jean-Yves Scoazec, Mathieu Coppey, Raphaël Voituriez, Matthieu Piel, and Fanny Jaulin. Cell clusters adopt a collective amoeboid mode of migration in confined non-adhesive environments. *Science Advances*, 8(39), September 2022. ISSN 2375-2548. doi:10.1126/sciadv.abp8416.

[6] Ana Rubio Denniss, Thomas E. Gorochowski, and Sabine Hauert. An open platform for high-resolution light-based control of microscopic collectives. *Advanced Intelligent Systems*, 4(7), May 2022. ISSN 2640-4567. doi:10.1002/aisy.202200009.

[7] Neshika Wijewardhane, Ana Rubio Denniss, Matthew Uppington, Helmut Hauser, Thomas E. Gorochowski, Eugenia Piddini, and Sabine Hauert. Long-term imaging and spatio-temporal control of living cells using light. In *2022 International Conference on Manipulation, Automation and Robotics at Small Scales (MARSS)*, page 1–6. IEEE, July 2022. doi:10.1109/marss55884.2022.9870487.

[8] Jason P. Town and Orion D. Weiner. Local negative feedback of rac activity at the leading edge underlies a pilot pseudopod-like program for amoeboid cell guidance. *PLOS Biology*, 21(9):e3002307, September 2023. ISSN 1545-7885. doi:10.1371/journal.pbio.3002307.

[9] Josiah B. Passmore, Alfredo Rates, Jakob Schröder, Menno T. P. van Laarhoven, Vincent J. W. Hellebrekers, Henrik G. van Hoef, Antonius J. M. Geurts, Wendy van Straaten, Wilco Nijenhuis, Florian Berger, Carlas S. Smith, Ihor Smal, and Lukas C. Kapitein. Outcome-driven microscopy: Closed-loop optogenetic control of cell biology. December 2024. doi:10.1101/2024.12.12.628240.

[10] Arthur Edelstein, Nenad Amodaj, Karl Hoover, Ron Vale, and Nico Stuurman. Computer control of microscopes using µmanager. *Current Protocols in Molecular Biology*, 92(1), October 2010. ISSN 1934-3647. doi:10.1002/0471142727.mb1420s92.

[11] GitHub - pymmcore-plus/pymmcore-plus: Pure python/C++ micro-manager ecosystem — github.com. https://github.com/pymmcore-plus/pymmcore-plus. [Accessed 25-03-2025].

[12] Jannis Ahlers, Daniel Althviz Moré, Oren Amsalem, Ashley Anderson, Grzegorz Bokota, Peter Boone, Jordão Bragantini, Genevieve Buckley, Alister Burt, Matthias Bussonnier, Ahmet Can Solak, Clément Caporal, Draga Doncila Pop, Kira Evans, Jeremy Freeman, Lorenzo Gaifas, Christoph Gohlke, Kabilar Gunalan, Hagai Har-Gil, Mark Harfouche, Kyle I. S. Harrington, Volker Hilsenstein, Katherine Hutchings, Talley Lambert, Jessy Lauer, Gregor Lichtner, Ziyang Liu, Lucy Liu, Alan Lowe, Luca Marconato, Sean Martin, Abigail McGovern, Lukasz Migas, Nadalyn Miller, Hector Muñoz, Jan-Hendrik Müller, Christopher Nauroth-Kreß, Juan Nunez-Iglesias, Constantin Pape, Kim Pevey, Gonzalo Peña-Castellanos, Andrea Pierré, Jaime Rodríguez-Guerra, David Ross, Loic Royer, Craig T. Russell, Gabriel Selzer, Paul Smith, Peter Sobolewski, Konstantin Sofiiuk, Nicholas Sofroniew, David Stansby, Andrew Sweet, Wouter-Michiel Vierdag, Pam Wadhwa, Melissa Weber Mendonça, Jonas Windhager, Philip Winston, and Kevin Yamauchi. napari: a multi-dimensional image viewer for python, 2023.

[13] Josh Moore, Daniela Basurto-Lozada, Sébastien Besson, John Bogovic, Jordão Bragantini, Eva M. Brown, Jean-Marie Burel, Xavier Casas Moreno, Gustavo de Medeiros, Erin E. Diel, David Gault, Satrajit S. Ghosh, Ilan Gold, Yaroslav O. Halchenko, Matthew Hartley, Dave Horsfall, Mark S. Keller, Mark Kittisopikul, Gabor Kovacs, Aybüke Küpcü Yoldaş, Koji Kyoda, Albane le Tournoulx de la Villegeorges, Tong Li, Prisca Liberali, Dominik Lindner, Melissa Linkert, Joel Lüthi, Jeremy Maitin-Shepard, Trevor Manz, Luca Marconato, Matthew McCormick, Merlin Lange, Khaled Mohamed, William Moore, Nils Norlin, Wei Ouyang, Bugra Özdemir, Giovanni Palla, Constantin Pape, Lucas Pelkmans, Tobias Pietzsch, Stephan Preibisch, Martin Prete, Norman Rzepka, Sameeul Samee, Nicholas Schaub, Hythem Sidky, Ahmet Can Solak, David R. Stirling, Jonathan Striebel, Christian Tischer, Daniel Toloudis, Isaac Virshup, Petr Walczysko, Alan M. Watson, Erin Weisbart, Frances Wong, Kevin A. Yamauchi, Omer Bayraktar, Beth A. Cimini, Nils Gehlenborg, Muzlifah Haniffa, Nathan Hotaling, Shuichi Onami, Loic A. Royer, Stephan Saalfeld, Oliver Stegle, Fabian J. Theis, and Jason R. Swedlow. Ome-zarr: a cloud-optimized bioimaging file format with international community support. *Histochemistry and Cell Biology*, 160(3):223–251, July 2023. ISSN 1432-119X. doi:10.1007/s00418-023-02209-1.

[14] Lucien Hinderling, Guillaume Witz, Roman Schwob, Ana Stojiljkovic, Maciej Dobrzynski, Mykhailo Vladymyrov, Joel Frei, Benjamin Graedel, Agne Frismantiene, and Olivier Pertz. Convpaint - universal framework for interactive pixel classification using pretrained neural networks. September 2024. doi:10.1101/2024.09.12.610926.

[15] Uwe Schmidt, Martin Weigert, Coleman Broaddus, and Gene Myers. Cell detection with star-convex polygons. In *Medical Image Computing and Computer Assisted Intervention - MICCAI 2018 - 21st International Conference, Granada, Spain, September 16-20, 2018, Proceedings, Part II*, pages 265–273, 2018. doi:10.1007/978-3-030-00934-2_30.

[16] Carsen Stringer and Marius Pachitariu. Cellpose3: one-click image restoration for improved cellular segmentation. *Nature Methods*, 22(3):592–599, February 2025. ISSN 1548-7105. doi:10.1038/s41592-025-02595-5.

[17] Imaging Server Kit — github.com. https://github.com/Imaging-Server-Kit. [Accessed 23-03-2025].

[18] Daniel B. Allan, Thomas Caswell, Nathan C. Keim, Casper M. van der Wel, and Ruben W. Verweij. soft-matter/trackpy: v0.6.4, 2024.

[19] Kristina Ulicna, Giulia Vallardi, Guillaume Charras, and Alan R. Lowe. Automated deep lineage tree analysis using a bayesian single cell tracking approach. *Frontiers in Computer Science*, 3:92, 2021. ISSN 2624-9898. doi:10.3389/fcomp.2021.734559.

[20] GitHub - pymmcore-plus/useq-schema: An implementation agnostic schema for describing a sequence of events during a multi-dimensional imaging acquisition. — github.com. https://github.com/pymmcore-plus/useq-schema. [Accessed 25-03-2025].

[21] Max Heydasch, Lucien Hinderling, Jakobus van Unen, Maciej Dobrzynski, and Olivier Pertz. Gtpase activating protein dlc1 spatio-temporally regulates rho signaling. December 2023. doi:10.7554/elife.90305.1.

[22] Linda Van Aelst and Crislyn D'Souza-Schorey. Rho gtpases and signaling networks. *Genes amp; Development*, 11(18):2295–2322, September 1997. ISSN 1549-5477. doi:10.1101/gad.11.18.2295.

[23] Kent L Rossman, Channing J Der, and John Sondek. Gef means go: turning on rho gtpases with guanine nucleotide-exchange factors. *Nature reviews Molecular cell biology*, 6(2):167–180, 2005.

[24] Paul M. Müller, Juliane Rademacher, Richard D. Bagshaw, Celina Wortmann, Carolin Barth, Jakobus van Unen, Keziban M. Alp, Girolamo Giudice, Rebecca L. Eccles, Louise E. Heinrich, Patricia Pascual-Vargas, Marta Sanchez-Castro, Lennart Brandenburg, Geraldine Mbamalu, Monika Tucholska, Lisa Spatt, Maciej T. Czajkowski, Robert-William Welke, Sunqu Zhang, Vivian Nguyen, Trendelina Rrustemi, Philipp Trnka, Kiara Freitag, Brett Larsen, Oliver Popp, Philipp Mertins, Anne-Claude Gingras, Frederick P. Roth, Karen Colwill, Chris Bakal, Olivier Pertz, Tony Pawson, Evangelia Petsalaki, and Oliver Rocks. Systems analysis of rhogef and rhogap regulatory proteins reveals spatially organized rac1 signalling from integrin adhesions. *Nature Cell Biology*, 22(4):498–511, March 2020. ISSN 1476-4679. doi:10.1038/s41556-020-0488-x.

[25] Jing Hoon, Mei Tan, and Cheng-Gee Koh. The regulation of cellular responses to mechanical cues by rho gtpases. *Cells*, 5(2):17, April 2016. ISSN 2073-4409. doi:10.3390/cells5020017.

[26] William M. Bement, Andrew B. Goryachev, Ann L. Miller, and George von Dassow. Patterning of the cell cortex by rho gtpases. *Nature Reviews Molecular Cell Biology*, 25(4): 290–308, January 2024. ISSN 1471-0080. doi:10.1038/s41580-023-00682-z.

[27] Catherine D Nobes and Alan Hall. Rho, rac, and cdc42 gtpases regulate the assembly of multimolecular focal complexes associated with actin stress fibers, lamellipodia, and filopodia. *Cell*, 81(1):53–62, April 1995. ISSN 0092-8674. doi:10.1016/0092-8674(95)90370-4.

[28] Katrin Martin, Andreas Reimann, Rafael D. Fritz, Hyunryul Ryu, Noo Li Jeon, and Olivier Pertz. Spatio-temporal co-ordination of rhoa, rac1 and cdc42 activation during prototypical edge protrusion and retraction dynamics. *Scientific Reports*, 6(1), February 2016. ISSN 2045-2322. doi:10.1038/srep21901.

[29] Ankita Jha, Ankit Chandra, Payam Farahani, Jared Toettcher, Jason M. Haugh, and Clare M.

Waterman. Cd44 and ezrin restrict egf receptor mobility to generate a novel spatial arrangement of cytoskeletal signaling modules driving bleb-based migration. January 2025. doi:10.1101/2024.12.31.630838.

[30] Jean De Seze, Maud Bongaerts, Benoit Boulevard, and Mathieu Coppey. Optogenetic control of a gef of rhoa uncovers a signaling switch from retraction to protrusion. February 2025. doi:10.7554/elife.93180.3.

[31] Vasundhara Rao, Benjamin Grädel, Lucien Hinderling, Jakobus Van Unen, and Olivier Pertz. Feedback regulation by the rhoa-specific gef arhgef17 regulates actomyosin network disassembly. August 2024. doi:10.1101/2024.08.28.610052.

[32] Artur Ruppel, Dennis Wörthmüller, Vladimir Misiak, Manasi Kelkar, Irène Wang, Philippe Moreau, Adrien Méry, Jean Révilloud, Guillaume Charras, Giovanni Cappello, Thomas Boudou, Ulrich S Schwarz, and Martial Balland. Force propagation between epithelial cells depends on active coupling and mechano-structural polarization. *eLife*, 12, August 2023. ISSN 2050-084X. doi:10.7554/elife.83588.

[33] Karsten Kruse, Rémi Berthoz, Luca Barberi, Anne-Cécile Reymann, and Daniel Riveline. Actomyosin clusters as active units shaping living matter. *Current Biology*, 34(20): R1045–R1058, October 2024. ISSN 0960-9822. doi:10.1016/j.cub.2024.08.043.

[34] William M. Bement, Marcin Leda, Alison M. Moe, Angela M. Kita, Matthew E. Larson, Adriana E. Golding, Courtney Pfeuti, Kuan-Chung Su, Ann L. Miller, Andrew B. Goryachev, and George von Dassow. Activator–inhibitor coupling between rho signalling and actin assembly makes the cell cortex an excitable medium. *Nature Cell Biology*, 17(11):1471–1483, October 2015. ISSN 1476-4679. doi:10.1038/ncb3251.

[35] Marko Šoštar, Maja Marinović, Vedrana Filić, Nenad Pavin, and Igor Weber. Oscillatory dynamics of rac1 activity in dictyostelium discoideum amoebae. *PLOS Computational Biology*, 20(12):e1012025, December 2024. ISSN 1553-7358. doi:10.1371/journal.pcbi.1012025.

[36] Benjamin Grädel, Lea Brönnimann, Paolo Armando Gagliardi, Lucien Hinderling, Olivier Pertz, and Maciej Dobrzyński. Tracking coordinated cellular dynamics in time-lapse microscopy with arcos.px. March 2025. doi:10.1101/2025.03.14.643386.

[37] Jonathan B. Michaux, François B. Robin, William M. McFadden, and Edwin M. Munro. Excitable rhoa dynamics drive pulsed contractions in the early c. elegans embryo. *Journal of Cell Biology*, 217(12):4230–4252, October 2018. ISSN 1540-8140. doi:10.1083/jcb.201806161.

[38] Ani Michaud, Marcin Leda, Zachary T. Swider, Songeun Kim, Jiaye He, Jennifer Landino, Jenna R. Valley, Jan Huisken, Andrew B. Goryachev, George von Dassow, and William M. Bement. A versatile cortical pattern-forming circuit based on rho, f-actin, ect2, and rga-3/4. *Journal of Cell Biology*, 221(8), June 2022. ISSN 1540-8140. doi:10.1083/jcb.202203017.

[39] Jonathan A. Jackson, Marlis Denk-Lobnig, Katherine A. Kitzinger, and Adam C. Martin. Change in rhogap and rhogef availability drives transitions in cortical patterning and excitability in drosophila. *Current Biology*, 34(10):2132–2146.e5, May 2024. ISSN 0960-9822. doi:10.1016/j.cub.2024.04.021.

[40] Rupamanjari Majumder, Iolanda Feola, Alexander S Teplenin, Antoine AF de Vries, Alexander V Panfilov, and Daniel A Pijnappels. Optogenetics enables real-time spatiotemporal control over spiral wave dynamics in an excitable cardiac system. *eLife*, 7, September 2018. ISSN 2050-084X. doi:10.7554/elife.41076.

[41] Naoya Hino, Leone Rossetti, Ariadna Marín-Llauradó, Kazuhiro Aoki, Xavier Trepat, Michiyuki Matsuda, and Tsuyoshi Hirashima. Erk-mediated mechanochemical waves direct collective cell polarization. *Developmental Cell*, 53(6):646–660.e8, June 2020. ISSN 1534-5807. doi:10.1016/j.devcel.2020.05.011.

[42] Sebastian Junge, Maria Elena Ricci Signorini, Masa Al Masri, Jan Gülink, Heiko Brüning, Leon Kasperek, Monika Szepes, Mine Bakar, Ina Gruh, Alexander Heisterkamp, and Maria Leilani Torres-Mapa. A micro-led array based platform for spatio-temporal optogenetic control of various cardiac models. *Scientific Reports*, 13(1), November 2023. ISSN 2045-2322. doi:10.1038/s41598-023-46149-1. "Sweeping lines and spirals, 16x16 px resolution".

[43] Coralie Dessauges, Jan Mikelson, Maciej Dobrzyński, Marc-Antoine Jacques, Agne Frismantiene, Paolo Armando Gagliardi, Mustafa Khammash, and Olivier Pertz. Optogenetic actuator – erk biosensor circuits identify mapk network nodes that shape erk dynamics. *Molecular Systems Biology*, 18(6), June 2022. ISSN 1744-4292. doi:10.15252/msb.202110670.

[44] Leone Rossetti, Steffen Grosser, Juan Francisco Abenza, Léo Valon, Pere Roca-Cusachs, Ricard Alert, and Xavier Trepat. Optogenetic generation of leader cells reveals a force–velocity relation for collective cell migration. *Nat. Phys.*, 20(10):1659–1669, October 2024. Similar to our approach, use NOA61 as photo polymerizing resin and DMD (PRIMO, Alvéole) for patterning.

[45] Kevin Suh, Richard Thornton, Payam E. Farahani, Daniel Cohen, and Jared Toettcher. Large-scale control over collective cell migration using light-controlled epidermal growth factor receptors. May 2024. doi:10.1101/2024.05.30.596676.

[46] Maciej Dobrzyński, Benjamin Grädel, Paolo Armando Gagliardi, and Olivier Pertz. Quantification of collective signalling in time-lapse microscopy images. *Methods in Microscopy*, 1 (1):19–30, April 2024. ISSN 2942-3899. doi:10.1515/mim-2024-0003.

[47] Paolo Armando Gagliardi, Maciej Dobrzyński, Marc-Antoine Jacques, Coralie Dessauges, Pascal Ender, Yannick Blum, Robert M. Hughes, Andrew R. Cohen, and Olivier Pertz. Collective erk/akt activity waves orchestrate epithelial homeostasis by driving apoptosis-induced survival. *Developmental Cell*, 56(12):1712–1726.e6, June 2021. ISSN 1534-5807. doi:10.1016/j.devcel.2021.05.007.

[48] Lucien Hinderling, Remo Hadorn, Moritz Kwasny, Joël Frei, Benjamin Grädel, Sacha Psalmon, Yannick Blum, Rémi Berthoz, Alex E. Landolt, Benjamin D. Towbin, Daniel Riveline, and Olivier Pertz. Teach your microscope how to print: low-cost and rapid-iteration microfabrication for biology. *Lab on a Chip*, 25(16):4091–4105, 2025. ISSN 1473-0189. doi:10.1039/d5lc00181a.

[49] Henry Pinkard and Laura Waller. Microscopes are coming for your job. *Nature Methods*, 19 (10):1175–1176, September 2022. ISSN 1548-7105. doi:10.1038/s41592-022-01566-4.

[50] Maxim A Ziatdinov, Ayana Ghosh, and Sergei V Kalinin. Physics makes the difference: Bayesian optimization and active learning via augmented gaussian process. *Machine Learning: Science and Technology*, 3(1):015003, February 2022. ISSN 2632-2153. doi:10.1088/2632-2153/ac4baa.

[51] Maxim A. Ziatdinov, Yongtao Liu, Anna N. Morozovska, Eugene A. Eliseev, Xiaohang Zhang, Ichiro Takeuchi, and Sergei V. Kalinin. Hypothesis learning in automated experiment: Application to combinatorial materials libraries. *Advanced Materials*, 34(20), April 2022. ISSN 1521-4095. doi:10.1002/adma.202201345.

[52] Stefanie Tellex, Nakul Gopalan, Hadas Kress-Gazit, and Cynthia Matuszek. Robots that use language. *Annual Review of Control, Robotics, and Autonomous Systems*, 3(1):25–55, May 2020. ISSN 2573-5144. doi:10.1146/annurev-control-101119-071628.

[53] Michael Ahn, Anthony Brohan, Noah Brown, Yevgen Chebotar, Omar Cortes, Byron David, Chelsea Finn, Chuyuan Fu, Keerthana Gopalakrishnan, Karol Hausman, Alex Herzog, Daniel Ho, Jasmine Hsu, Julian Ibarz, Brian Ichter, Alex Irpan, Eric Jang, Rosario Jauregui Ruano, Kyle Jeffrey, Sally Jesmonth, Nikhil J Joshi, Ryan Julian, Dmitry Kalashnikov, Yuheng Kuang, Kuang-Huei Lee, Sergey Levine, Yao Lu, Linda Luu, Carolina Parada, Peter Pastor, Jornell Quiambao, Kanishka Rao, Jarek Rettinghouse, Diego Reyes, Pierre Sermanet, Nicolas Sievers, Clayton Tan, Alexander Toshev, Vincent Vanhoucke, Fei Xia, Ted Xiao, Peng Xu, Sichun Xu, Mengyuan Yan, and Andy Zeng. Do as i can, not as i say: Grounding language in robotic affordances, 2022.

[54] Danny Driess, Fei Xia, Mehdi S. M. Sajjadi, Corey Lynch, Aakanksha Chowdhery, Brian Ichter, Ayzaan Wahid, Jonathan Tompson, Quan Vuong, Tianhe Yu, Wenlong Huang, Yevgen Chebotar, Pierre Sermanet, Daniel Duckworth, Sergey Levine, Vincent Vanhoucke, Karol Hausman, Marc Toussaint, Klaus Greff, Andy Zeng, Igor Mordatch, and Pete Florence. Palm-e: An embodied multimodal language model, 2023.

[55] João Pedro Fonseca, Alain R. Bonny, G. Renuka Kumar, Andrew H. Ng, Jason Town, Qiu Chang Wu, Elham Aslankoohi, Susan Y. Chen, Galen Dods, Patrick Harrigan, Lindsey C. Osimiri, Amy L. Kistler, and Hana El-Samad. A toolkit for rapid modular construction of biological circuits in mammalian cells. *ACS Synthetic Biology*, 8(11):2593–2606, November 2019. ISSN 2161-5063. doi:10.1021/acssynbio.9b00322.

# Methods

## Cell culture

All cell lines were cultured at 37°C with 5% $CO_2$ **NIH3T3 cells:** *Culture conditions.* NIH3T3 cells were maintained in:

- DMEM high-glucose
- 5% fetal bovine serum
- 4 mM L-glutamine
- 200 U/ml penicillin
- 200 µg/ml streptomycin

*Imaging conditions.* Imaging experiments were performed in a starving medium consisting of:

- DMEM high-glucose
- 0.5% BSA (Sigma)
- 200 U/ml penicillin
- 200 µg/ml streptomycin
- 4 mM L-glutamine

**MCF10A cells:** *Culture conditions.* MCF10A human mammary cells were maintained in:

- DMEM:F12
- 5% horse serum
- 20 ng/ml recombinant human EGF (Peprotech)
- 10 µg/ml insulin (Sigma)
- 0.5 µg/ml hydrocortisone (Sigma)
- 200 U/ml penicillin
- 200 µg/ml streptomycin

*Imaging conditions.* Imaging experiments were performed in a starving medium:

- DMEM:F12
- 0.3% BSA
- 0.5 µg/ml hydrocortisone
- 200 U/ml penicillin
- 200 µg/ml streptomycin

**optoLARG MCF10A cells:** Tet-inducible optoLARG MCF10A cells were cultured in the presence of 1000 ng/mL doxycycline for 72 hours to induce transgene expression. Culture medium was replaced every 24 hours with fresh medium containing doxycycline. After 48 hours, Growth medium was exchanged to starvation medium for the remaining 24 hours.

**REF52** / **NIH3T3 Cells:** *Culture conditions.* Rat Embryo Fibroblast 52 (REF52) and mouse embryonic Fibroblasts (NIH3T3) cells were maintained in Dubelcco's Modified Eagle (DMEM) with:

- DMEM high-glucose
- 10% 4 mM L-glutamine
- 100 U/ml penicillin/streptomycin

*Imaging conditions.* Cells were incubated in FluoroBrite DMEM overnight.

## Imaging

*Cell seeding.* NIH3T3 and REF52 cells were seeded in 96-well 1.5H glass-bottom plates (Cellvis) coated with 10 µg/ml Fibronectin (Huber lab) at a density of $1.5 \times 10^3$ cells/well and incubated for 24 h. MCF10A cells were seeded in 24-well 1.5H glass-bottom plates (Cellvis) coated with 5 µg/ml Fibronectin (Huber lab) at $1 \times 10^5$ cells/well and incubated for 48 h.

*Imaging Setup.* Imaging was performed using an automated Eclipse Ti inverted fluorescence microscope (Nikon) with a Plan Apo air 20x, air 40x, oil 60x objective. The Nikon Perfect Focus System (PFS) was

used to maintain focus. Illumination was provided by a SPECTRA X LED light engine (Lumencor) with the following filters (Chroma):

- **mCitrine:** 508 nm LED, ET500/20×, 69308bs, ET535/30m.
- **mRuby2 and dTomato:** 555 nm LED, ET575/25×, 69008bs, 59022m.
- **miRFP703:** 640 nm LED, ET640/30×, 89100bs Sedat Quad, 84101m Quad.

DMD devices used were Andor Mosaic 3 and Mightex Polygon 1000. Images were acquired using an Andor Zyla 4.2 plus camera at a 16-bit depth.

### Plasmids and cell lines

**optoLARG, 2xrGBD, lifeact, paxillin in REF52:** constructs and cell line generation for REF52 experiments (pB3.0-optoLARG-mVenus-SspB-p2A-stargazin-mtq2-iLID, mCherry-paxillin, dTomato-2xrGBD, lifeact miRFP) are described in [21]

**optoFGFR, ERK-KTR, H2B in MCF10A and NIH3T**: The optogenetic actuator/biosensor circuit for activating and reading ERK activity (optoFGFR, ERK-KTR-mRuby2, H2B-miRFP) and stable cell line generation are described in [43].

**optoTIAM** REF52 cell lines were stably transfected with CAG-optoTIAM-mVenus-iLID-nano.

**optoLARG, ERK-KTR, H2B**: MCF10A cell lines were stably transfected with constitutively expressed CAG-ErkKTR-mRuby2-P2A-H2B-miRFP703 and Tet-inducible pTRE-sspB-mNeongreen-LARG-pTRE-Stargazin-mTurquoise2-iLID-CAG-Tet-ON.

**optoTrkA, ERK-KTR, H2B in NIH3T3**: Cell line was stably co-transfected through the PiggyBac transposon system with a transposase plasmid and a plasmid containing PGK1-optoTrkA-mCitrine, CAG-ERKKTR-mScarlet3, CAG-H2B-miRFP670nano3 and CAG-Lifeact-miRFP670nano3. The construct was assembled by modular cloning using the Mammalian Tool Kit (MTK) [55], with additional parts domesticated to include optoTrkA, Lifeact, mScarlet3, and miRFP670nano3.

*Cell selection post-transfection.*

- Puromycin (P7255, Sigma)
- Blasticidin S HCl (5502, Tocris)
- Hygromycin B (sc-29067, Lab Force)